Paleo-Earthquakes along the Zheduotang Fault, Xianshuihe Fault System, Eastern Tibet: Implications for Seismic Hazard Evaluation

Guifan Chen [*1, 2], **Mervin Bartholomew**[3], **Demin Liu**[1], **Kai Cao**[1], **Minxuan Feng**[4], **Dun Wang**[1]

1. *School of Earth Sciences, China University of Geosciences, Wuhan* 430074, *China*
2. *Three Gorges Geotechnical Consultants Co., Ltd., Wuhan* 430074, *China*
3. *Department of Earth Sciences, University of Memphis, TN* 38152, *USA*
4. *Xi' an Center of Geological Survey, China Geological Survey, Xi' an* 710054, *China*
Guifan Chen: https://orcid.org/0000-0002-1313-7685

ABSTRACT: The Kangding City in eastern Tibet is at high risk due to frequent strong earthquakes along the Xianshuihe sinistral strike-slip fault bounding the Chuandian Block to the northeast. The knowledge of paleo-seismicity recurrence along this fault system is key to the evaluation of earthquake hazards in this region; thus, more accurate paleoseismic information are required. We examined the paleo-seismicity along the Zheduotang fault in the central segment of the Xianshuihe fault system by applying the field investigation, trenching, and Quaternary dating methods (e.g., OSL and ¹⁴C). Field observations found ~8.5 m offset of stream by sinistral slip along the Zheduotang fault. We trenched the central fault zone of the Zheduotang fault and found that the colluvial wedges and five buried, discontinuous, A-soil horizons progressively have been offset in the shallow graben on the SW-side of the main fault indicative of the paleo-earthquakes. The dating results of OSL and ¹⁴C, in line with existing data, enable us to establish the paleo-seismic history of the Zheduotang fault. It shows at least eight surface ruptures in the last 7500 years identified from displaced buried soils, colluvial wedges and terraces. Our study reveals ~100 years minimum paleo-earthquake recurrence, suggesting potential large earthquakes in the Kangding area in the future.
KEY WORDS: Tibetan Plateau, Xianshuihe fault system, paleo-seismicity, trench, recurrence, geophysics.

0　INTRODUCTION

The ongoing collision between the India and Eurasia plates is one of the most significant tectonic events since the Phanerozoic, resulting in uplift of the Tibetan Plateau and thickening of the underlying crust (e.g., Wang S Y et al., 2021; Wang S F et al., 2008; Yin, 2006; Tapponnier and Molnar, 1997; Wang and Burchfiel, 2000). Normal to the collisional zone, large-scale horizontal movement across the Tibetan Plateau account for markedly asymmetric growth of topography towards the east, and for large amounts of both localized sinistral shear and coeval, distributed crustal thickening (e. g., Tapponnier et al., 2001, 1982), contrasting with the lower crustal flow that predicts limited crustal shortening in eastern Tibet (e. g., Clark and Royden, 2000; Royden et al., 1997). Inherent in developing new ideas about evolution of the Tibetan Plateau, is establishing relationships among tectonic features (e. g., active

faults, strong earthquakes, plutonism and metamorphism) and geomorphic features (uplift and erosion). As an important part of northeastern boundary of the Tibetan Plateau, the Xianshuihe fault system characterized by left-lateral oblique strike-slip faults has experienced frequent large earthquakes, such as 1973 M7.6, 1967 M7.0, 1955 M7.5, 1816 $M7^1/_2$, and 1786 $M7^3/_4$ (Fig. 1). Thus, many geologists have systematically studied its activity and seismicity to help explore the motion mechanism of the Tibetan Plateau and to evaluate past and future seismic hazards.

From the vicinity of Qianning to Moxi, the Xianshuihe fault system curves southward, with a gradual change in the strikes from ~140° to ~160°, forming a relay transition transition from the Yalahe, through the Selahe and Zheduotang faults, to the Moxi fault, while a newly discovered fault-Mugecuo South fault lies between the Selaha fault (SLH F.) and Zheduotang fault (ZDT F.) (Figs. 1b, 2a) (Bai et al., 2021), which makes the tectonic activity and geomorphological features in this area more complex. The 1955 M7.5 Zheduotang earthquake, occurred along the Zheduotang fault (ZDT F.) near Kangding City, is the most recent earthquake larger than M7 that attracts the attention of many geologists. Previous geological studies mainly focused on three aspects of the Zheduotang fault: (1) geometric characteristics, e.g., fault length and strike


(Ma, 2020; Liang, 2019; Chen, 2006); (2) kinematic characteristics, e.g., slip and uplift (Bai et al., 2021, 2018; Yan et al., 2019; Zhang et al., 2009; Tapponnier et al., 2001); and (3) paleoseismic events and recurrence periods (Cheng et al., 2011; Papadimitriou et al., 2004).

However, due to the remoteness and inaccessibility of the study area, recurrence periods are not well determined yet to evaluate the potential earthquakes in the near future, e.g., only a few large events were identified via a limited number of trenches (Ma et al., 2020; Zhou et al., 2001; Li et al., 1997). Thus, more detailed earthquake events and recurrence periods of the Zheduotang fault need to be identified, as well as the potential seismic hazard in the city of Kangding which is inhabitazed by a moderate population of ~126 000 and where part of the planned route of the Sichuan-Tibet Railway passes through

(Bai et al., 2021).

Here we provide new geomorphological, sedimentological, and structural characteristics of the Zheduotang fault where co-seismic surface rupture occurred during the 14 April 1955 *M*7.5 Zheduotang earthquake. Terraces and offsets of Holocene alluvial fans indicate that frequent, episodic strike-slip displacement accompanied uplift associated with surface fractures and landslides in the epicentral area of the 14 April 1955 *M*7.5 Zheduotang earthquake. Optically Stimulated Luminescence (OSL) and calibrated ¹⁴C (calBCE/CE) dates from our trench (CUG-2013-1), combined with results from an earlier trench (Zhou et al., 2001) across the Zheduotang fault, and from fluvial deposits and terraces provides a paleoseismic history dating back to the Late Pleistocene in this area.
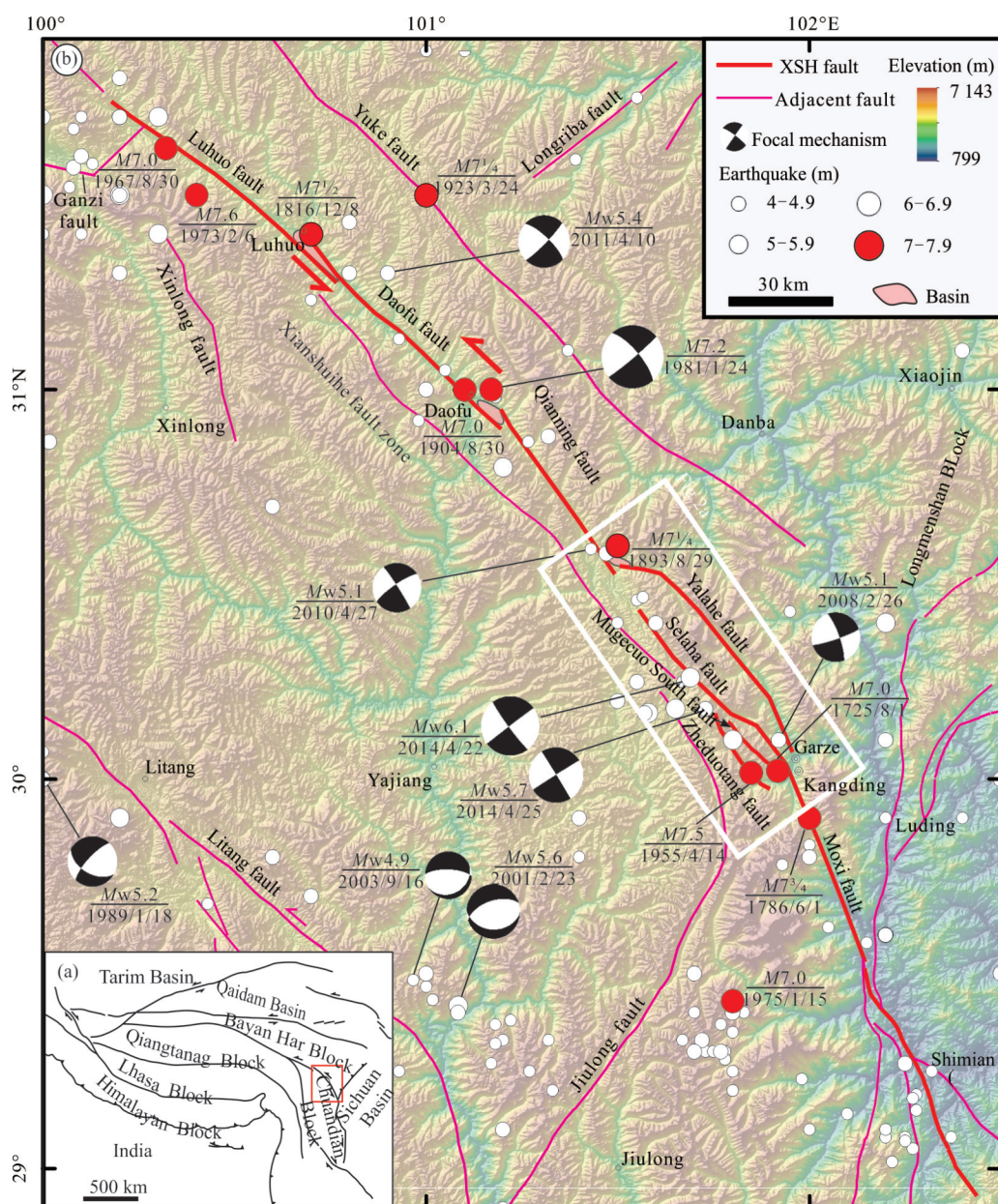
Figure 1. (a) Tectonic map showing principal faults of Tibet and adjacent regions; (b) comprehensive map of Xianshuihe fault zone with earthquakes of magnitude ≥*M*4.0 (from China Earthquake Catalogue) (Cao et al., 2019). Focal mechanism solutions are from the Global CMT catalogue (https://www.globalcmt.org/).

1 GEOLOGICAL SETTING

The 350 km-long, NW-trending Xianshuihe strike-slip fault zone bounds the Chuandian Block to the northeast. The fault system consists of seven segments which are Luhuo, Daofu, Qianning, Yalahe, Selaha, Zheduotang, and Moxi faults from north to south (Chen et al., 2016; An, 2010; Allen et al., 1991). The formation and evolution of this fault system is closely related to the expansion process of the Tibetan Plateau (Zhang et al., 2017). Rupture activity history and sliding rates are both somewhat controversial (Bai et al., 2021; Tang et al., 2021). Recent studies suggested that the fault zone has experienced three main stages of tectonic evolution since the Cenozoic (Tang et al., 2021; Li et al., 2015; Li and Zhang, 2013; Zhang et al., 2015): (1) ca. 32–25 Ma, the onset stage of left lateral slip; (2) ca. 20–13 Ma, the peak deformation period of a strong left lateral ductile shear and large-scale magmatism, e.g., Zheduoshan Batholith; (3) ca. 10 Ma–present, brittle left-lateral strike-slip accommodating block rotation and enhanced seismic activity. Chen et al. (2020) considered the initial activation of the Xianshuihe fault zone to be no later than 47 Ma and that large-scale leftward slip occurred from 5 Ma onward. Blocked by the Bayan Har Block, Longmenshan Block and Sichuan Basin, the slip rate along the Xianshuihe fault system thus increases to the SE from 6–8 mm/yr along the Ganzi fault, to 8–11 mm/yr along the NW Xianshuihe fault, to 8–12 mm/yr along the SE Xianshuihe fault, to 9.6–13.4 mm/yr along the

Moxi fault (Fig. 2a)(Bai et al., 2021, 2018).

The Zheduotang fault is more than 30 km long with an overall trend of ~325° (Fig. 2b) (Chen, 2006). Zheduo Mountain Pass marks a change from a NE-dip to a SW-dip to the northeast. Recent study by Ma (2020) suggested that the main fault of the ZDT F. is a strike-slip reverse fault that continues to the northwest for about 16 km from the Kangding Airport, while Liang (2019) found that the ZDT F. continues to the SE to the Yajiageng pass through field mapping and high-resolution remote sensing images. Furthermore, the ZDT F. composed of a series of small right-stepping, en-echelon segments (Zhang and Xie, 2001) developed across moraine sediments on the gentle southwestern slope of Zheduo Mountain, offsetting a series of gullies with a SW-dip fault scarp in the opposite direction to the slope (Fig. 2b). In the southeast part, however, it cut a succession of ridges and produced landforms such as side-slope ridges, fault valleys and sag ponds (e.g.,Yan et al., 2019, 2018; Yin et al, 2010).

Although the slip rate of ZDT F. is relatively slow compared to the Selaha fault and Moxi fault both in Late Quaternary timescale and geodetic timescale (Bai et al., 2021), seismic activity of ZDT F. appears to be no weaker than the other two faults. Geomorphic characteristics are complex because the incised Zheduo River cuts deeply across the landscape preserving remnants of the graben, offset channels, terraces, and fault scarps.
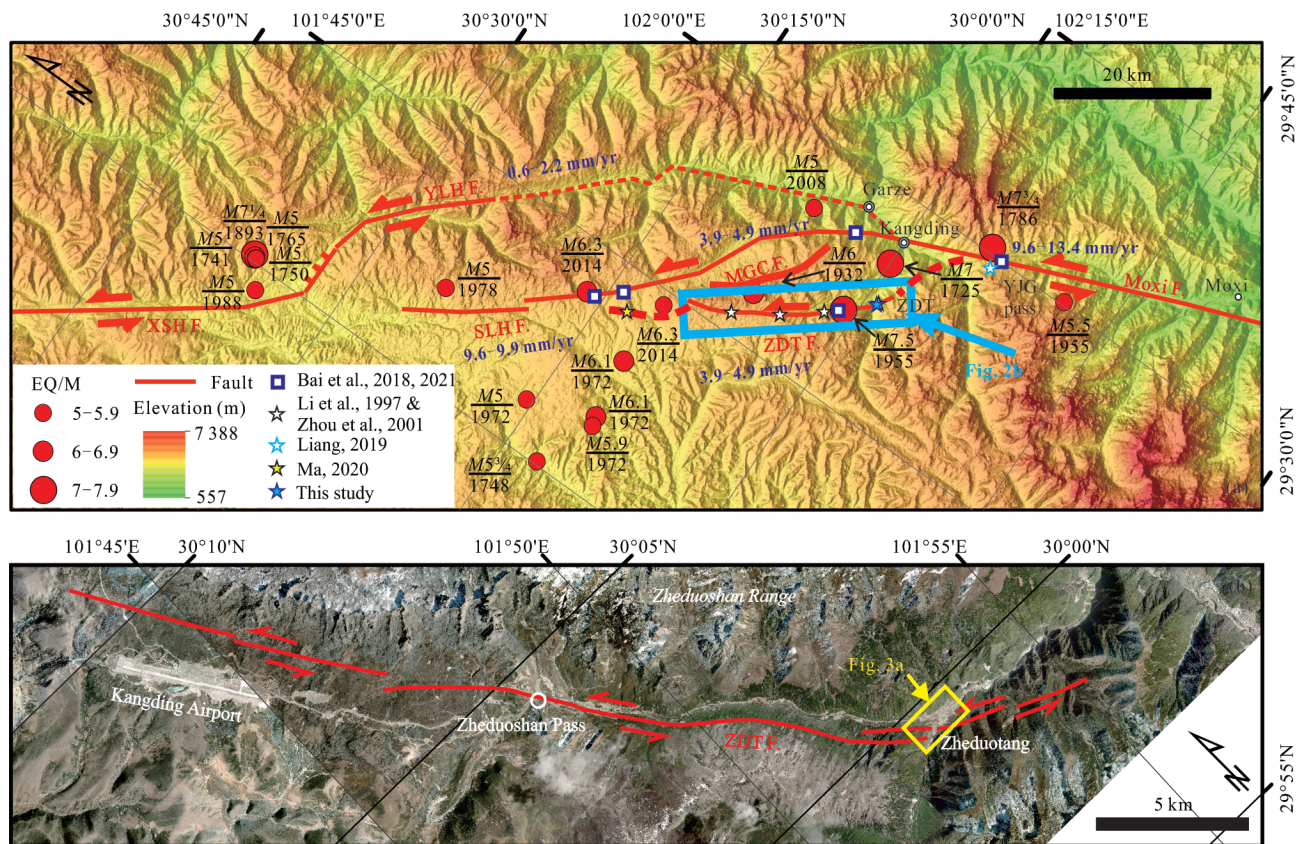
Figure 2. (a) Structural activity of the Xianshuihe fault system in the Kangding area; (b) remote sensing map of the Zheduotang fault from Google Earth. Slip rates in dark blue is from Bai et al. (2021). XSH F. Xianshuihe fault; YLH F. Yalahe fault; SLH F. Selaha fault; ZDT F. Zheduotang fault; MGC F. Mugecuo South fault; YJG. Yajiageng.

2 SAMPLING AND METHODS

We used field investigation, Google Earth satellite images and topographic data to map the faults, terraces, alluvial fans to choose an appropriate trenching site. Then we dug our trench (Trench CUG2013-1) across the ZDT F. where a small graben lied in front of a Holocene alluvial fan.

We used the method of ^{14}C dating to determine the age of Late Quaternary soils where plant fossils or other reliable carbon materials are absent (Wang et al., 1996), despite the fact that the mean residence time (Jenkinson and Rayner, 1977) can be influenced by unknown proportions of old or young organic carbon compounds in the soil organic carbon pool (Martin and Johnson, 1995). A total of 17 ^{14}C samples were collected in the trench profiles and terraces. AMS ^{14}C dating was done in the School of Archaeology and Museology in Peking University. The half-life of ^{14}C is 5 568 yr and BP represent time before 1950. Most of the ^{14}C samples from trench CUG2013-1 are paleosoil with an exception of a piece of charcoal. While all the ^{14}C ages turn out to be buried ages, the charcoal may provide direct proof of a forest fire relating with extreme drought. For terraces, samples were collected just below the A soil-horizon and show inferred ages of when that terrace formed. However, because of influences from certain degrees of anthropogenic modifications, the ^{14}C dating results should be used cautiously. Only six of the thirteen ^{14}C ages were used in our terrace analysis and are listed in Table 1. The other 7 samples were excluded from our analysis because of contamination by modern soil.

To compensate for the missing ages, we collected some more Optically Stimulated Luminescence (OSL) samples for dating, while OSL is a method for measuring doses from ionizing radiation and helps in defining the age of fluvial deposits (e. g., Murray and Olley, 2002). We collected an OSL sample from Trench CUG2013-1 (Table 2 KD2013-1). It is from the bottom of the stream sediments with bedded gravels, which are likely late Pleistocene alluvial fan deposits. In contrast, an OSL sample from terrace deposits from the bottom of the Old Trench

Table 1 ^{14}C age for Trench CUG2013-1, Old Trench 2000, and terraces

Sample	Description	Locality from Fig. 4	^{14}C date yrs. BP [a]	$2\sigma s$ yrs. [a]	^{14}C Calibrated calendar age (BCE/CE) [b]	2σ [b]
KD201310-14C-3	Trench A1 soil-horizon paleosol	13	100	20	1800-1930calCE	69.1%
KD201310-14C-4	Trench A2 soil-horizon paleosol	13	3 095	25	1424-1288calBCE	95.4%
KD201310-14C-5	Trench A4 soil-horizon paleosol	13	3 860	20	2459-2281calBCE	90.1%
KD201310-14C-6	Trench A5 soil-horizon paleosol	13	6 565	30	5561-5477calBCE	91.3%
KD201310-14C-7	Terrace 4 paleosol	3	2 945	25	1260-1050calBCE	
KD201310-14C-9	Alluvial fan	8	350	30	1462-1635calCE	
KD201310-14C-10	Terrace 2 paleosol	9	2 030	25	111calBCE-30calCE	93.1%
KD201310-14C-11	Terrace 1 paleosol	10	100	20	1800-1930calCE	
KD201310-14C-12	Alluvial fan	7	505	20	1405-1430calCE	95.4%
KD201310-14C-17	Terrace 1 paleosol	6	110	30	1802-1938calCE	65.5%
OT2000-14C-1[c]	OT2000 A1 soil-horizon paleosol	14	1215	70	669-908calCE	85.2%
OT2000-14C-2[c]	OT2000 A2 soil-horizon paleosol	14	2 695	150	1220-415calBCE	95.4%
OT2000-14C-3[c]	OT2000 A3? soil-horizon paleosol	14	1 600	80	316-615calCE	90.6%
OT2000-14C-4[d]	soil-horizon, Graben fillings		2 700	150	1226-416calBCE	95.4%
OT2006-14C-5[e]	soil-horizon, Graben fillings	4	2 338	28	486-366calBCE	95.4%
OT2019-14C-1[f]	FDZR in roadcut (detrital carbon)	5	8 540	40		

a. Radiocarbon ages from AMS (Accelerator Mass Spectrometry) are referenced to the year 1950 CE. Analytical uncertainties are reported at 2σ.

b. Dendrochronologically calibrated calendar age by Bayesian plot method from OxCal v4.3.2 Ramsey (2017) and IntCal 13 atmospheric curve (Reimer et al., 2013). c. Ages are from Trench dug in (or before) 2000 reported by Zhou et al., 2001.

d. Age is from soil sample reported by Zhou et al., 2001. e. Age is from Chen, 2006. f. Age is from Yan et al., 2019.

g. CE is an abbreviation for Common Era and BCE is short for Before Common Era. CE and BCE are used in exactly the same way as the traditional abbreviations AD and BC.

Table 2 OSL ages for Trench CUG2013-1, old Trench 2000, and terraces

| Sample	Description	Depth (m)	Locality from Fig. 4	OSL age (ka)	2σ (ka)	OSL AGE (BCE/CE) with 2σ from Fig. 3
KD2013-1	Fluvial sediment in south end of Trench CUG2013-1	1.30	12	18.25	1.5	18250 BCE+/-1500 yrs
KD2016-3	T5 (main terrace) Ancient river	0.10	1	8.1	1.7	6084 BCE+/-1700 yrs
KD2016-9	T5 near Loc. 2	0.60	2	8.0	0.9	5984 BCE+/-900 yrs
KD2016-12	Bank of Zheduo River	0.50		0.8	0.1	1216 CE+/-100 yrs
KD2016-15	Prominent knob along fault	0.50		10.3	1.2	8284 BCE+/-1200 yrs
KD2016-16	New age (2016) from old trench (2000) below A-2	0.60	11	8.2	0.7	6084 BCE+/-700 yrs

2000 (Zhou et al., 2001) are of mid-Holocene age (Table 2, KD2016-16). Three OSL samples were collected from terraces north of the trench (KD2016-3, 9, 12) while the last one was collected on the hill near the ZDT F. to the south of the trench (KD2016-15). The OSL samples were tested in the Photoluminescence Dating Laboratory, China University of Geosciences (Wuhan) in 2016. The instrument used for the test was the Danish RisφTL/OSL-DA-20, with a feldspar signal excitation source of 830 nm IR light and a quartz signal excitation using blue light (470 ± 20 nm) at 130 ℃ for 40 s. The irradiation source was 90-Sr/90-Y beta (at a given dose). We used single aliquto regenerative protocols (SAR) for determination of equivalent dose (De) and used the common growth curve (CGC) method to determinate the De (Lai and Ou, 2013).

3 RESULTS AND INTERPRETATION

3.1 Geomorphic Features along the Zheduotang Fault

Human reconstructive activities, infrequent structural offsets of the Zheduo River channel across the Zheduotang fault zone, and larger-scale climatic and/or regional tilting, uplift/incision rates may all affect how the fluvial terraces of the Zheduo River are mapped and dated. Approximately five terraces were recognized by field investigation and remote high-resolution topographic data in the confluence of Zheduo River and Maojia River (Figs. 3 and 4). Upstream from the fault zone, the younger, paired T1, T2, and T3 terraces parallel the river and exhibit larger area sizes with each riser possessing a height of 1–2 m in average and are partially bordered by larger granitoid boulders used to level the fields. Smaller, irregularity scattered, granitic boulders and cobbles which appear to be deposits from Cenozoic debris flows from the hillslopes down on-
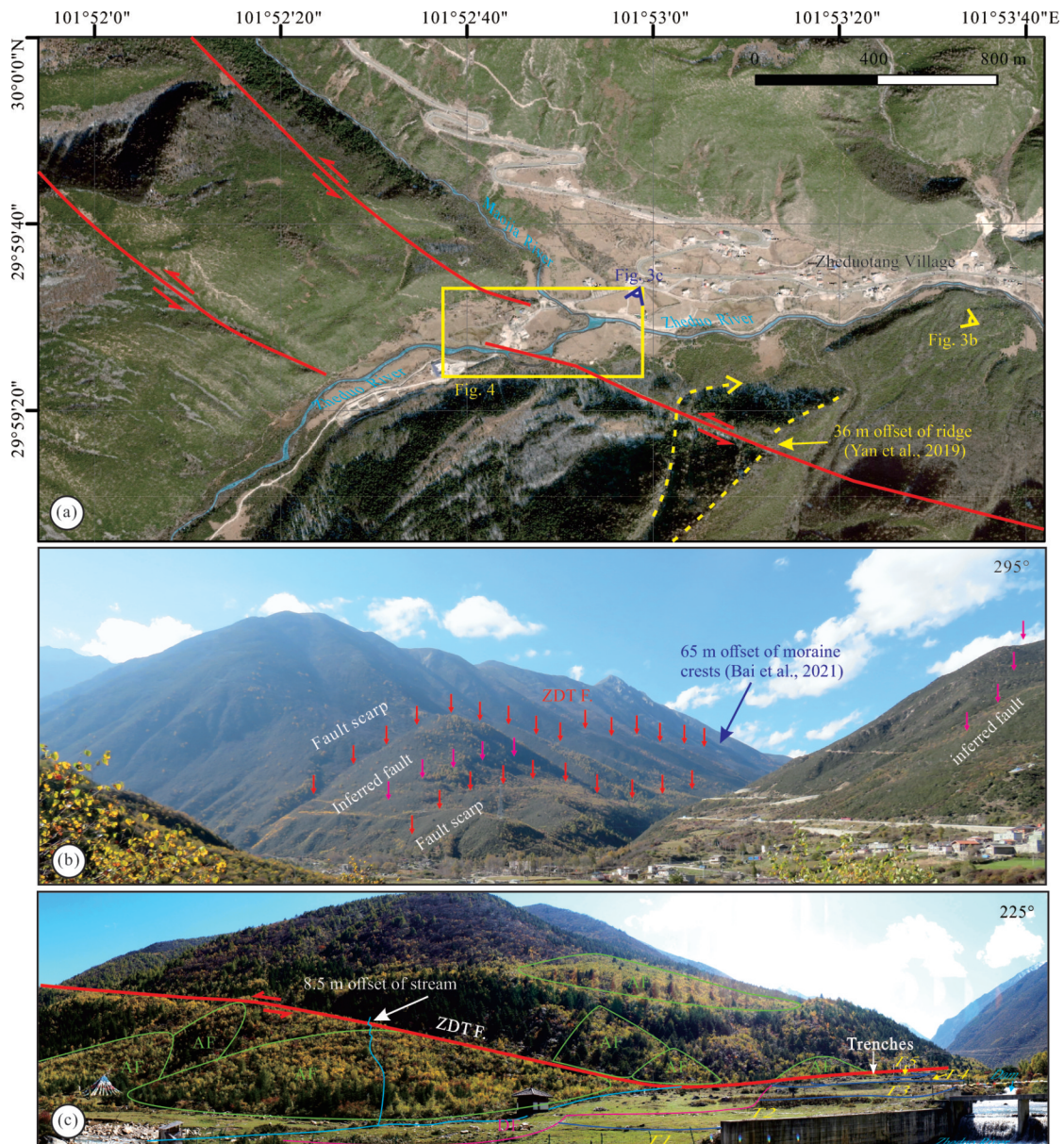
Figure 3. (a) Zheduotang fault and Zheduo River in the Zheduotang area; (b) photo of the Zheduotang fault face to NW of the Zheduotang village; (c) photo of the Zheduotang fault and terraces face to the SW. AF. alluvial fan; DF. debris flow.

to the terraces (Figs. 3c and 4). Downstream from the fault zone, T1-T4 terraces are more perpendicular to the Zheduo River, suggesting the southeast-flowing Maojia River tributary and tributaries from the mountainous northern flank of the Zheduo River played a significant part in shaping the landscape near the merger of these rivers. Two ages of T1 pin down its development at ~1800–1938 CE (Fig. 4, Loc. 6 and 10; Table 1) before the 1955 CE Zheduotang earthquake. The uplifting of terraces are coordinated with the compressive effect between the en-chelon segments of right stepping, left-lateral Zheduotang fault zone (Figs. 3 and 4).

Along the Zheduotang fault on the hills in the southern side of the valley, a series of alluvial fans formed during the Late Pleistocene to Holocene, along the Zheduo River (Fig. 3c). Approximately 0.37 km SE of the river along the fault, a narrow, NE-trending stream valley is sharply deflected 8.5 m left-laterally before it sharply returns to its NE-trending flow at the apex of a well-developed Holocene–Late Pleistocene alluvial fan. The OSL age around the knob of the alluvial fan and the fault is 10.3 ± 1.0 ka (Table 2) and such offset leads to a very low slip rate along the Zheduotang fault since the Late Pleistocene. Periodic large earthquakes along the Xianshuihe fault zone are consistent with a long history of displacement along it, but different researchers have estimated a wide range in displacement-rates along different part of the zone. Zhou et al. (2001) used a ^{14}C age and the displacement of the first terrace to calculate the strike-slip rate of Zheduotang fault as 3.5 ± 0.3 mm/a since the Holocene. Chen (2006) used two ^{14}C ages from two terraces near Zheduo River to calculate the strike-slip rate of the Zheduo fault to be as 8.5 ± 2 mm/a. Yan et al. (2019) measured 36 meters of left-lateral offset of a late Quaternary terrace riser which they interpreted as the total slip on the Zheduotang fault and estimated the slip rate to be 3.4 ± 0.4 mm/yr. Bai et al. (2021) obtained 65 ± 10 m offsets of the ZDT moraines and ^{10}Be ages ranging from 12.7 ± 1.0 to 30.0 ± 2.4 ka, yield a left-lateral slip-rate of 4.1 ± 0.7 mm/yr.

3.2 Trench CUG2013-1 and the 2000 Trench (Zhou et al., 2001)

The Zheduotang fault zone occurs in a highly vegetative area, hence morphology of fluvial and alluvial deposits that are cut by the fault zone are difficult to decipher. Trenching is a practical option to resolve some subsurface deformation along active faults. We chose to trench across the trace of the main fault zone with a small graben between the alluvial fan and terraces to maximize the likelihood of obtaining datable material indicative of surface ruptures during earthquakes. Trenching proximal to the Zheduo River's floodplain, necessarily limits the depth of the paleoseismic record of buried A horizons, colluvial wedges, and progressive offsets to the Holocene. These two separate shallow trenches (Figs. 5c, 5d, and 5g) had a total length of 25 meters and an ~1.4 m gap separates them to avoid damage to a through-going buried plastic pipe.

Zhou et al. (2001) dug a small trench (labeled as Zhou et al., 2001, Trench, 2000, in Fig. 4, Loc. 11) across a terrace and the flank of a small graben along the Zheduotang fault. They recognized several apparent normal faults that cut the A-soil horizon consistent with surface rupture during the 1955 earthquake (Figs. 5a, 5b). We examined several meters of the exposed upper end of that old trench 2000, redrew that trench profile, and distinguished A1a, A1b? and A2? horizons based on the weathering characteristics they described. Also, some collapse and fill fissures were marked alongside faults which are consistent with older surface ruptures. The big, rounded granite boulder lying between the NE-dipping and the SW-dipping faults, is typical of the FDZR (Fig. 4). An OSL sample collected from the bottom of the Trench 2000 (Fig. 5, Loc. 11) in 2016 (6084 BCE+/-800 yrs) demonstrates that it correlates with T5 (Fig. 4, Loc. 1; 6084 BCE +/-1700 yrs).
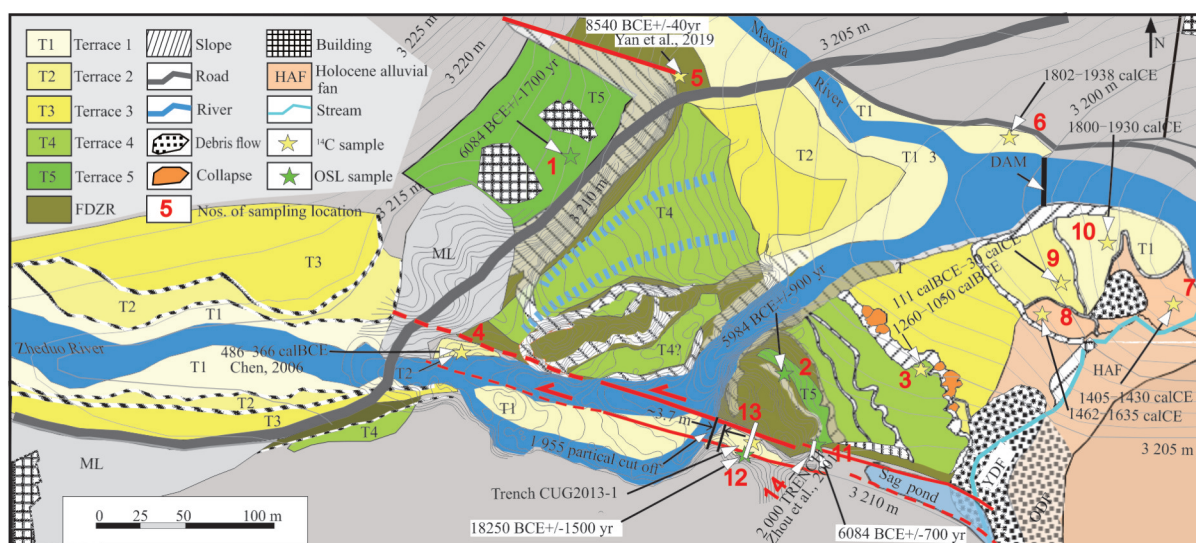
Figure 4. Map of Quaternary features in the area where the Zheduo River crosses the Zheduotang fault zone (red lines) showing fault-bounded graben, Holocene terraces (T1, T2, T3, T4, T5), locality numbers with OSL and calBCE/CE ^{14}C ages at those localities, trench locations (white bars), ODF. older debris flow; YDF. younger debris flow; HAF. Holocene alluvial fan; ML. modified land; B. building; FDZR. stripped areas-escarpments. DEM contour lines from Google Earth and Chen, 2006.

3.2.1 Stratigraphic section from trench CUG2013-1

Multiple buried A soil-horizons in trench CUG2013-1, indicate progressive burial in the graben after earthquakes. In trench CUG2013-1, we identified the A/O horizon, the B horizon and several buried A horizons in the graben-sediments. The thicknesses of A soil-horizons are slightly different with A1: 20 cm, A2: 20 cm, A3: 15 cm, A4: 20 cm, and A5: 15 cm (Figs. 5c, 5d, and 5g). The small graben contains discontinuous lenses of A horizons with cobbles, surrounded with clay, suggesting small colluvial wedges slid down into small sag ponds along the main fault (Fig. 4). Today, many cobbles and boulders are distributed on the ground surface alongside the curved river and graben-slope consistent with surface shaking during the 1955 earthquake. Soil samples from A1, A2, A4 and A5, that have ^{14}C ages (Fig. 5, Loc. 15–18) consistent with burial ages when cobbles slide down small escarpments during ancient earthquakes along the Zheduotang fault. Each event may indicate a surface rupture (Lindvall et al., 2002; McGill and Rockwell, 1998) correlative with landslides or debris flows, and/or river offsets as well. The record of these events, e.g., numerous cobbles or pebbles disperse in the mud in A2 or A3 are widely distributed in the trenches and are associated with small displacements on the faults (Fig. 5).

3.2.2 Analysis of trench CUG2013-1 and the 2000 trench (Zhou et al., 2001)

What is obvious from the trench logs (Fig. 5) is that different types of faults (e.g., oblique-reverse F3 and F13, oblique-normal F4 and F6, thrust F11 and F15) indicate a typical Riedel fracture array consistent with a transpressional fault zone near the Zheduo River. Bedding in the NE part of the north trench (Figs. 5c, 5d and 5e) shows that fluvial deposits of the Zheduo River (FDZR) were displaced by apparent normal and reverse faults on both the SE and NW walls. Three parallel S-dipping high-angle normal faults are on the northern trench-wall. The strata contain cobbles supported with a sandy loam matrix. Most cobbles are granitic with sizes ranging from ~3 to ~20 cm. All these cobbles are consistent with a source from the FDZR where apparent normal faults are most likely caused by uplift of the terraces as well. Considering the lithologic contrasts between bedded FDZR deposits in trench CUG2013-1 and multiple colluvial wedges and sag-pond deposits, the fault F3 on the north flank of the graben is interpreted as the major strike-slip fault separating graben sediments from FDZR deposits (Figs. 5c, 5d). The old trench was dug across T5 (Fig. 4, Loc. 14), downward across the main fault into graben fill. The very large, rounded, granitic boulder (at 3–4.2 m horizontal distance) is clearly part of the FDZR as are the enveloping and overlying units. Although Zhou et al. (2001) did not identify the main fault (probably because of a lack of contrast in sediments of units 3 and 4) in the old trench, the main fault likely broke the surface during the 1955 earthquake at 5.2 m (F3, Fig. 5a), adjacent to the small boulder there.

Some overall features that are apparent when looking at the trench logs are

(1) Only a thin veneer of soil occurs at the NE end of CUG2013-1.

(2) FDZR spacing the terraces near the trenches indicates ongoing relative uplift and erosion relative to subsidence, deposition, and soil formation in the shallow graben.

(3) The age of sediment in the SW end (Fig. 6, Loc. 2) of CUG2013-1 also indicates considerable ongoing uplift relative to the graben, with thrust faults (Fig. 5) being a clear indicator of transpression.

Besides, it is notable that most of Trench 2000 lies about two meters below the level of CUG2013-1 making it difficult to correlate comparable soils/units, which is thought to be caused by differences in depositional environments.

3.3 Age Estimation of a Soil-Horizons

All but one of the dated ^{14}C samples and the estimated ages of the base of some buried A soil-horizons do lie near the median lines of the Bayesian ordered precision envelopes that readily show the youngest two breaks in the depositional/soil-formation records (~2 400 BCE to ~900 CE; and ~1 200 CE-present day; Fig. 6) between dated material. Thus, they are useful in interpreting some geological history.

We used ^{14}C ages and approximate thicknesses of A soil-horizons near those sample locations to estimate the age of the base of each A soil-horizon, assuming a constant rate of soil formation during the Holocene (Fig. 5, Loc. 16–21). Thus, the Bayesian ordering of dated samples (Fig. 6) from: (1) buried A soil-horizons; (2) small colluvial wedges; (3) approximated ages of the base of A soil-horizons; and (4) terraces coupled with incremental displacements of soil horizons, constrain the timing of surface ruptures some earthquakes experienced that disrupted the soil-formation system.

The significance of a sequence of buried A soil-horizons in the graben, lies in the understanding that

(1) The base of each represents the timing of sufficient vertical displacement that a large earthquake triggered to re-shape the slope and fault-bounded walls of the graben.

(2) Thus, producing the A1 and A2 horizons (Fig. 5) that thin and pinch out over uplifted, eroded FDZR on the N-end of the graben where many small faults terminate upward against the base of these two soil horizons.

(3) On both sides of the N-end of Trench 2013-1, only A1 overlies a thin B1 suggesting ~1 m of erosion has occurred over the FDZR knob after B1 had formed.

(4) On the S-end of the graben, an irregular mantle of the A1 and A2 soil-horizons capped the extensive, thick B1 horizon suggesting a long period of relative stability along most of the slope.

(5) But A2 upwardly terminated the very large displacement fault that cuts off B1 and older soils and sediments adjacent to the large alluvial fan deposits coming down the S-side of the large escarpment.

(6) In the central part of the graben, A3, A4, and A5 each developed contemporaneously with small colluvial wedges (like those in Fig. 5) adjacent to small faults.

3.4 Paleoearthquakes and Historical Earthquakes

The trench data (Fig. 5) with the Bayesian plot of OSL and calibrated ^{14}C ages in the 2σ-precision-envelope (Figs. 6a and 6b), gives our best approximation of the timing of surface ruptures occurred relative to the median line.
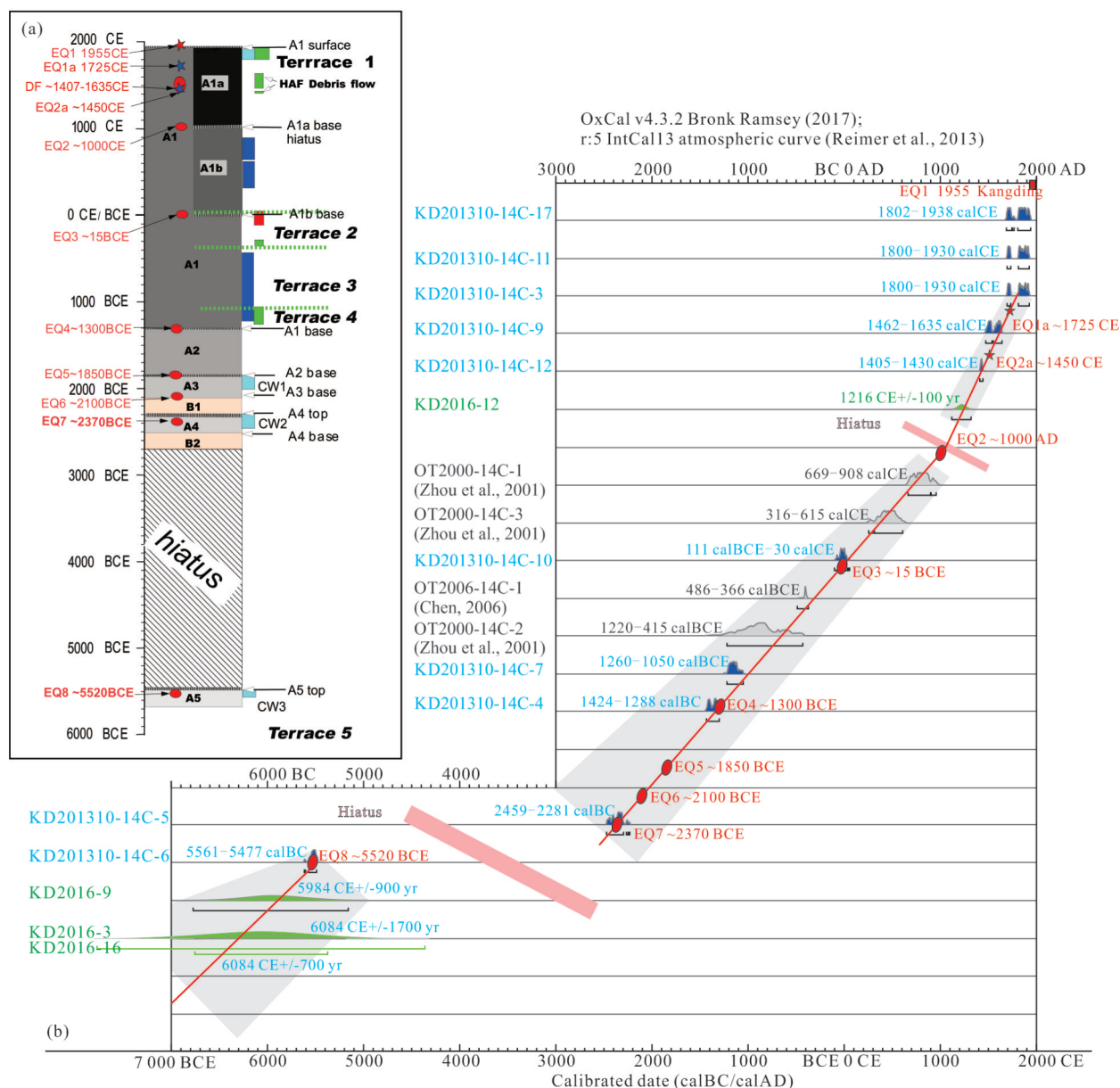
Figure 6. (a) Composite stratigraphic soil column showing approximate ages of the base of each soil that terminated faults or younger soils indicative surface rupture during earthquakes; (b) Bayesian plot of OSL and calBCE/calCE ^{14}C ages with 2σ precision envelopes with median lines illustrating significant breaks (hiatus) in the depositional/soil-formation record. The estimation of when some earthquakes occurred is based the presence of colluvial wedge material and/or change in soil-thickness change across fault-bounded blocks.

3.4.1 EQ1: M7.5 14 April 1955 Zheduotang earthquake

We have labeled as EQ1 those offsets that occurred in 1955 (as noted by Zhou et al., 2001) and typically offset or fold the A1 soil-horizon (dated at $1800-1930$ calCE) (Fig. 5, Loc. 16). EQ1 is identified at numerous points in both the trench log of trench 2000 and trench CUG2013-1 (Fig. 5), where the most recent movement of Zheduotang faults clearly show displacement during the 1955 M7.5 Zheduotang earthquake. Besides, another prominent evidence for the 1955 earthquake is ~3.7 m offset of the older river channel as shown in Fig. 4. Additionally, large granite boulders lie along the linear trend of the steep fault scarp suggesting strong ground motion there.

The thicknesses of older buried A soil-horizons provide a

way of estimating when earthquakes might have occurred by estimating the thickness between dated samples above and below each base of an A horizon along the median line of the 2σ-precision envelope. The top of A1 in the graben was dated at $1810-1925$ calCE (Fig. 5c, Loc. 16). That same A1 was uplifted ~1 m along four reverse faults during the 1955 earthquake (Fig. 5g, southern end of trench CUG2013-1) and preserved as a tectonic terrace T1 (Fig. 4). We assume that the top of A1a (Fig. 5a), which was also offset during EQ1 (the 1955 earthquake), has an equivalent age (~1810–1925 CE).

3.4.2 The Pre-1955 earthquake records in trenches

EQ1a: We found no indication of the 1725 CE (EQ1a on Fig. 6) earthquake which is consistent with Yan et al. (2019)
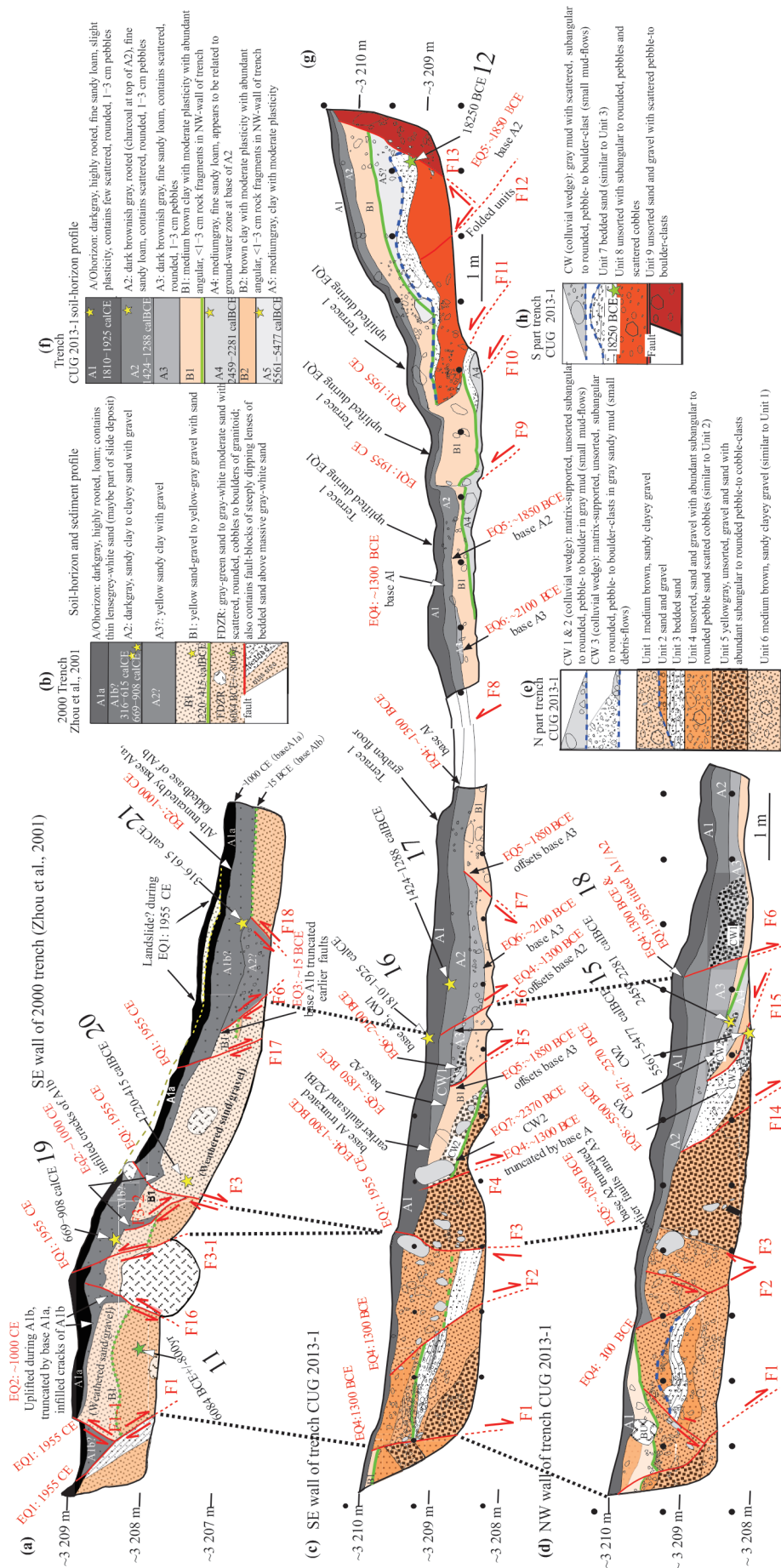
Figure 5. (a), (b) Old trench profile with calBCE/CE ages modified from Zhou et al. (2001); (c) SE wall of north trench CUG2013-1 with calBCE/CE ages; (d) NW wall of north trench CUG2013-1 with calBCE/CE ages; (g) SE wall of south trench CUG2013-1 calBCE/CE age; (f) soil-horizon profile of trench CUG2013-1. The distance between each two co-ordinate points is one meter for trench log (c), (d) and (g). Classification of soils in this paper used the Australian Soil and Land Survey Field Handbook (National Committee on Soil and Terrain, 2009). O soil-horizon: organic sur-face layer; may be strongly affected by human activity; A soil-horizon: surface soil layer with pronounced soil structure; composed of clay minerals and organic matters; B soil-horizon: subsoil layer with less organic matter and more clay than the A horizon.

and Chen et al. (2016) who showed "the severely damaged area" around the nearby Selaha fault was just a short distance farther east of CUG2013-1.

EQ2: Evidence for EQ2 is found in the trench 2000 (Zhou et al., 2001). The base of A1a formed after EQ2 over the irregular A1b horizon. Samples from near, but above, the base of A1b in the 2000 Trench (Fig. 5a, Locs. 19 and 21) provide age ranges of 316–908 CE for estimating an approximate age of ~15 BCE for A1b with the proportional thicknesses of A1a : A1b that places the age of A1a at ~1000 CE (Fig. 6a). Infilled cracks through the A1b surface (Fig. 5a, near Loc. 19) demonstrate that surface-faulting occurred during EQ2 (Zhou et al., 2001), thus EQ2 is estimated to have occurred ~1000 CE.

EQ2a: Although we found no evidence of EQ2a in the trenches, the young alluvial fan soils (Fig. 4, Locs. 7 and 8) with ages of 1407–1440 calCE and 1446–1635 calCE, are consistent with fine-grained sediment being winnowed out of the young debris flow of a similar age range to the 1414–1638 CE earthquake by Li et al. (1997). Thus, EQ2a has a probable age of ~1450 CE and may have been felt around region of the trench sites with serious side effects like landslides.

EQ3: Evidence of surface rupture during EQ3 is in the 2000 trench. The base of A1b developed after EQ3 when relative normal faulting occurred in the central part of the graben at ~15 BCE (Fig. 5A). Development of Terrace 2 may have ended around the time that the base of A1b was formed.

EQ4: We used the thickness A1 in the graben (Fig. 5c, Loc. 16) to the base of A1 near Loc. 17. A1 developed over a very uneven faulted A2 surface and truncates both A2 and B1 entirely in the uplifted northern end of Trench CUG2013-1 (Figs. 5c and 5d). These logs place the base of A1 at ~1300 BCE (Figs. 6a and 6b).

EQ5: The dated sample from near the top of A2 (Fig. 5c, Loc. 17) is 1424–1288 calBCE. The thickness of A2 near that location is similar to that of A1, hence the time equivalent is ~550 years which places the base of A2 at ~1850 BCE.

EQ6: Relative to the thicknesses of A1 and A2, the thickness of A3 is about half ~300 years which places the base of A3 with CW1 at ~2100 BCE (Figs. 5c and 5d).

EQ7: The dated sample of A4 with CW2 (Fig. 5d, Loc. 18) is 2459–2281 BCE, which places EQ7 at ~2370 BCE.

EQ8: The dated sample of A5 with CW3 (Fig. 5D, Loc. 15) is 5561–5477 BCE, which places EQ8 at ~5520 BCE.

4 DISCUSSION

Comparing with the paleoseismic events revealed by previous studies (Ma, 2020; Liang, 2019; Zhou et al., 2001; Li et al., 1997) near Zheduotang as shown in Fig. 7, the paleoseismic events obtained in this study are partially consistent with previous studies, e.g., EQ2a corresponding to E2, EQ7 corresponding to E6, EQ8 corresponding to E7, etc. (Fig. 7). The others can fill in the calendar of paleoseismic events of the ZDT F., which helps us to obtain more accurate earthquake recurrence cycles and understand the tectonic activity history of Zheduotang area.

Based on topography analyses of topography, deformed horizons exposed in the trenches, and calibrated ^{14}C dating ages, we inferred the occurrence of at least eight surface-

rupturing events on the Zheduotang fault in the last ~7500 years (EQ1–EQ8 in Figs. 5 and 6) which implies a minimum frequency of about 1000 years. Excluding EQ8 because of the large hiatus and including EQ2a which is reliable to some extent for its similarity with E2 (Fig. 7) (Li et al., 1997), then the average frequency for these eight earthquakes is about ~618 years. The earthquake events identified by previous studies from different sites along the ZDT F. since Holocene were ordered in the Time-events diagram (Fig. 7). According to this diagram, it is not hard to find that E3 and Z2, E4 and Z3, EQ5-EQ7 and E5 are in well correspondence respectively and all of the ages are dated by ^{14}C, indicating a better reliability of these results. Considering the ages' break between EQ1 and EQ2 in trench CUG2013-1, it will be more convincing to add other credible events in estimating the seismic recurrence of ZDT F. Thus, we add the ages of E3/Z2, E4/Z3 and L2 to our paleoseismic sequences for calculation (EQ1, EQ2a, EQ2, E3/Z3, E4/Z3, EQ3, EQ4, L2, EQ5, EQ6, EQ7), we can further pinpoint the average paleoseismic recurrence period to ~420-year since ~2370 BCE. The minimum recurrence interval between two events (EQ2 and E3/Z2) is ~100 yr, thus the Zheduotang fault has a possibility of strong earthquake occurring during the next hundred years because the last event occurred in 1955.

However, considering the discontinuity of the thin depositional/soil-forming record in the graben and the limited data obtained overall in this study, it is likely that identification of historic- and paleo-earthquakes is incomplete, particularly for large earthquakes that may have experience displacement at depth and/or tilting/uplift without obvious evidence of surface rupture. Hence, a recurrence rate less than 1 000 years is probable. The Bayesian plot (Fig. 6b) shows "thousand-year" gap, indicative a lack of datable material, interspersed with evidence of surface-ruptures every few hundred years (Fig. 6A). Thus, the compressed, discontinuous record in trenches likely contains many gaps in the earthquake record.

Since the seismic energy released by the 2014 M6.3 and M5.8 Kangding earthquake sequence is far less than the accumulated strain energy since the 1955 M7.5 earthquake on the ZDT F. (e.g., Xie et al., 2017; Jiang, et al., 2015a, b). The regional Coulomb stress increase following the 2008 Wenchuan (e.g., Nalbant and McCloskey, 2011) and 2013 Lushan (M7.0) (Guo et al., 2018; Yang et al., 2015) earthquakes implies that the seismic risk in the Kangding region has increased (Bai et al., 2021). Although the geometry of the YLH F., SLH F. and ZDT F. are juxtaposed, the fault strands at the surface may connect at depth (He et al., 2017). Thus, it is reasonable to suggest that the Kangding area is at a high risk of incurring large earthquakes in the future.

5 CONCLUSION

The conclusions are based on the results of topographic analyses, field investigations, and outcrop and trench excavations.

(1) Including the M7.5 14 April 1955 Zheduotang earthquake, Zheduotang fault is recognized as an active fault with at least eight surface ruptures since ~5500 BCE. Considering the ~3000-year hiatus between EQ8 and EQ7, the Zheduotang fault suggests an average paleoseismic recurrence of ~618
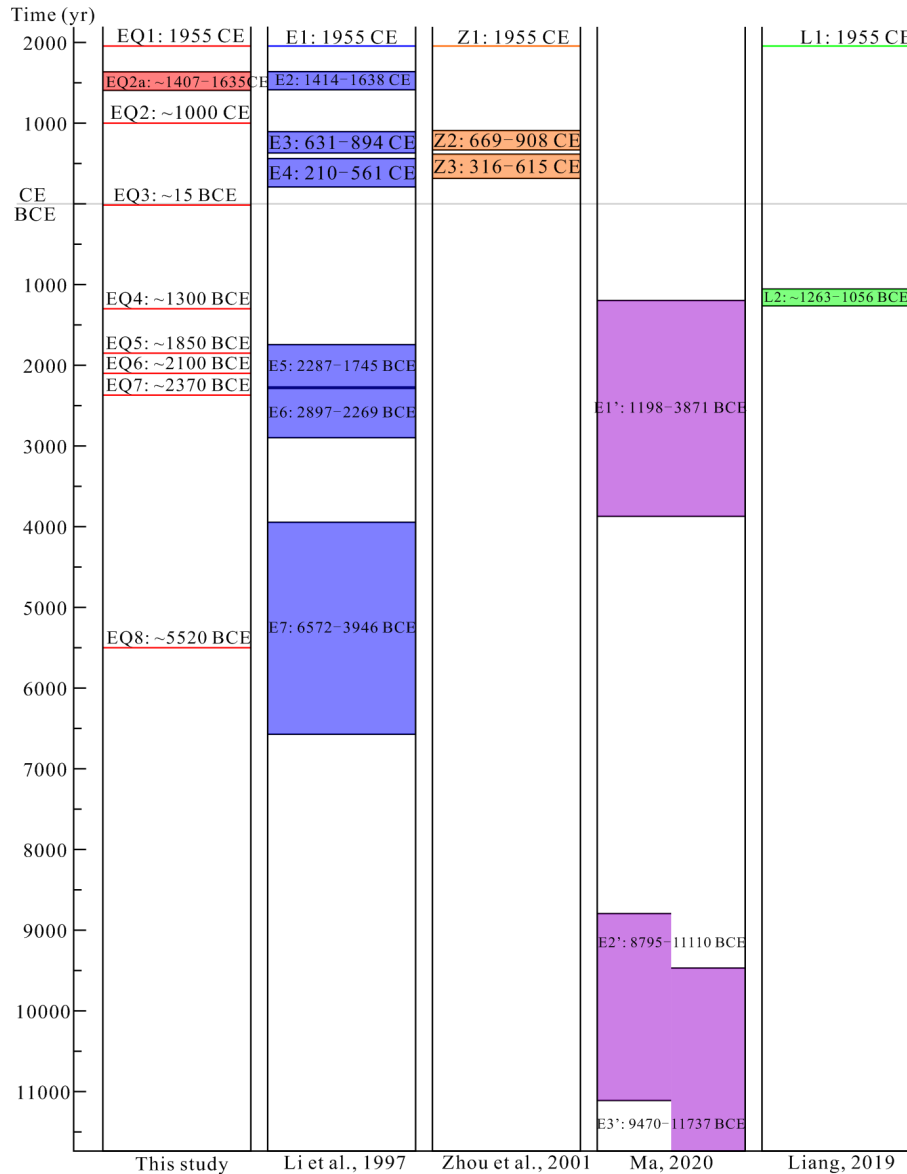
Figure 7. Holocene paleoseismic events in Zheduotang area.

years from EQ1 to EQ7. Adding the results of previous studies, we narrow the paleoseismic recurrence period to ~420-year since EQ7. However, considering the slow discontinuous accumulation of sediment and soil in the narrow, shallow graben, and the number of small faults along which we can show different times of displacement, we suspect the earthquake record is incomplete along this part of the fault zone. The average paleoseismic recurrence period is likely to be shorter than ~420-year.

(2) Combined with the previous studies of the study area, the minimum paleoseismic recurrence interval is about 100 yrs. Since the 1955 M7.5 earthquake on the ZDT F. over 60 years has passed, there is a high probability of strong earthquakes within the next 100 years. Otherwise, as more accumulated strain energy are to be released after the 2014 M6.3 and M5.8 earthquakes, the Kangding area is still in a high seismic risk.

ACKNOWLEDGMENTS

REFERENCE CITED

Allen, C. R., Luo, Z., Qian, H., et al., 1991. Field Study of a Highly Active Fault Zone: The Xianshuihe Fault of Southwestern China. *Geological Society of America Bulletin*, 103(9): 1178–1199

An, Y. F., 2010. Boundary Features of the Seismic Rupture Segments along the Xianshuihe Fault Zone: [Dissertation]. Institute of Geology, China Earthquake Administration, Beijing (in Chinese)

Bai, M. K., Chevalier, M. L., Leloup, P. H., et al., 2021. Spatial Slip Rate

Distribution along the SE Xianshuihe Fault, Eastern Tibet, and Earthquake Hazard Assessment. *Tectonics*, 40(11) https://doi.org/10.10 29/2021tc006985

Bai, M. K., Chevalier, M. L., Pan, J. W., et al., 2018. Southeastward Increase of the Late Quaternary Slip-Rate of the Xianshuihe Fault, Eastern Tibet. Geodynamic and Seismic Hazard Implications. *Earth and Planetary Science Letters*, 485(3–4): 19–31. https://doi.org/10.101 6/j.epsl.2017.12.045

Cao, K., Wang, G. C., Leloup, P. H., et al., 2019. Oligocene-Early Miocene Topographic Relief Generation of Southeastern Tibet Triggered by Thrusting. *Tectonics*, 38(1): 374–391. https://doi.org/10.1029/2017tc00 4832

Chen, G. H., 2006. Structural Transformation and Strain Partitioning along the Northeast Boundary Belt of the Sichuan-Yunnan Block: [Dissertation]. Institute of Geology, China Earthquake Administration, Beijing (in Chinese)

Chen, G. H., Xu, X. W., Wen, X. Z., et al., 2016. Late Quaternary Slip-Rates and Slip Partitioning on the Southeastern Xianshuihe Fault System, Eastern Tibetan Plateau. *Acta Geologica Sinica-English Edition*, 90(2): 537–554. https://doi.org/10.1111/1755-6724.12689

Chen, Y. T., Zhang, G. W., Lu, R. K., et al., 2020. Formation and Evolution of Xianshuihe Fault Belt in the Eastern Margin of the Tibetan Plateau: Constraints from Structural Deformation and Geochronology. *Geological Journal*, 55(12): 7953–7976

Cheng, J., Liu, J., Gan, W. J., et al., 2011. Characteristics of Strong Earthquake Evolution around the Eastern Boundary Faults of the Sichuan-Yunnan Rhombic Block. *Science China Earth Sciences*, 54: 1716(2011). https://doi.org/10.1007/s11430-011-4290-2

Clark, M. K., Royden, L. H., 2000. Topographic Ooze: Building the Eastern Margin of Tibet by Lower Crustal Flow. *Geology*, 28(8): 703–706. https://doi.org/10.1130/0091-7613(2000)28<703:tobtem>2.0.co;2

Guo, R. M., Zheng, Y., Tian, W., et al., 2018. Locking Status and Earthquake Potential Hazard along the Middle-South Xianshuihe Fault. *Remote Sensing*, 10(12): 2048. https://doi.org/10.3390/rs10122048

He, M. X., Fang, H., Wang, X. B., et al., 2017. Deep Conductivity Characteristics of the Southern Xianshuihe Fault Zone, Chinese. *Chinese Journal of Geophysics*, 60(6): 2414–2424 (in Chinese with English Abstract)

Jiang, G. Y., Wen, Y. M., Liu, Y. J., et al., 2015a. Joint Analysis of the 2014 Kangding, Southwest China, Earthquake Sequence with Seismicity Relocation and InSAR Inversion. *Geophysical Research Letters*, 42(9): 3273–3281. https://doi.org/10.1002/2015gl063750

Jiang, G. Y., Xu, X. W., Chen, G. H., et al., 2015b. Geodetic Imaging of Potential Seismogenic Asperities on the Xianshuihe-Anninghe-Zemuhe Fault System, Southwest China, with a New 3-D Viscoelastic Interseismic Coupling Model. *Journal of Geophysical Research: Solid Earth*, 120(3): 1855–1873. https://doi.org/10.1002/2014jb011492

Jenkinson, D. S., Rayner, J. H., 1977. The Turnover of Soil Organic Matter in some of the Rothamsted Classical Experiments. *Soil Science*, 171(1977): S130–S137. https://doi.org/10.1097/00010694-197705000-00005

Lai, Z. P., Ou, X. P., 2013. Basic Procedures of Optically Stimulated Luminescence (OSL) Dating. *Progress in Geography*, 32(5): 683–693

Li, H. L., Zhang, Y. Q., Zhang, C. H., et al., 2015. Middle Jurassic Syn-Kinematic Magmatism, Anatexis and Metamorphism in the Zheduo-Gonggar Massif, Implication for the Deformation of the Xianshuihe Fault Zone, East Tibet. *Journal of Asian Earth Sciences*, 107: 35–52. https://doi.org/10.1016/j.jseaes.2015.03.038

Li, H. L., Zhang, Y. Q., 2013. Zircon U-Pb Geochronology of the Konggar

Granitoid and Migmatite: Constraints on the Oligo-Miocene Tectono-Thermal Evolution of the Xianshuihe Fault Zone, East Tibet. *Tectonophysics*, 606(103): 127–139. https://doi.org/10.1016/j.tecto.201 3.07.007

Li, T. S., Du, Q. F., You, Z. L., et al., 1997. The Active Xianshuihe Fault Zone and Its Seismic Risk Assessment. Chengdu Cartographic Publishing House, Chengdu (in Chinese)

Liang, M. J., 2019. Characteristics of the Late-Quaternary Fault Activity of the Xianshuihe Fault: [Dissertation]. Institute of Geology, China Earthquake Administration, Beijing (in Chinese)

Lindvall, S. C., 2002. Evidence for Two Surface Ruptures in the Past 500 Years on the San Andreas Fault at Frazier Mountain, California. *Bulletin of the Seismological Society of America*, 92(7): 2689–2703. https://doi.org/10.1785/0120000610

Ma, J., 2020. Characteristics of the Late-Quaternary Fault Activity and Seismic Hazard of the Zheduotang Fault: [Dissertation]. Institute of Geology, China Earthquake Administration, Beijing (in Chinese). https://doi.org/10.27489/d.cnki.gzdds.2020.000006

Martin, C. W., Johnson, W. C., 1995. Variation in Radiocarbon Ages of Soil Organic Matter Fractions from Late Quaternary Buried Soils. *Quaternary Research*, 43(2): 232–237. https://doi.org/10.1006/qres.19 95.1023

McGill, S., Rockwell, T., 1998. Ages of Late Holocene Earthquakes on the Central Garlock Fault near El Paso Peaks, California. *Journal of Geophysical Research*: *Solid Earth*, 103(B4): 7265–7279. https://doi.org/10.1029/97jb02129

Murray, A. S., Olley, J. M., 2002. Precision and Accuracy in the Optically Stimulated Luminescence Dating of Sedimentary Quartz: A Status Review. *Geochronometria*, 21: 1–16

Nalbant, S. S., McCloskey, J., 2011. Stress Evolution before and after the 2008 Wenchuan, China Earthquake. *Earth and Planetary Science Letters*, 307(1–2): 222–232. https://doi.org/10.1016/j.epsl.2011.04.039

Papadimitriou, E., Wen, X., Karakostas, V., et al., 2004. Earthquake Triggering along the Xianshuihe Fault Zone of Western Sichuan, China. *Pure and Applied Geophysics*, 161: 1683–1707. https://doi.org/10.1007/s00024-003-2471-4

Ramsey, C. B., 2017. OxCal 4.3.2 Manual (Online): https://c14.arch.ox.ac.uk/oxcalhelp/hlp_contents.html

Reimer, P. J., Bard, E., Bayliss, A., et al., 2013. IntCal13 and Marine13 Radiocarbon Age Calibration Curves 0–50 000 Years Cal BP. *Radiocarbon*, 55(4): 1869–1887. https://doi.org/10.2458/azu_js_rc.5 5.16947

Tang, Y., Wang, P., Deng, H., et al., 2021. Petrological Records of Major Tectono-Magmatic Events since Oligocene in the Southeastern Segment of Xianshuihe Fault Zone in the Eastern Margin of Tibetan Plateau. *Geological Bulletin of China*, in press

Tapponnier, P., Molnar, P., 1977. Active Faulting and Tectonics in China. *Journal of Geophysical Research*, 82(20): 2905–2930. https://doi.org/10.1029/jb082i020p02905

Tapponnier, P., Peltzer, G., Le Dain, A. Y., et al., 1982. Propagating Extrusion Tectonics in Asia: New Insights from Simple Experiments with Plasticine. *Geology*, 10(12): 611–616. https://doi.org/10.1130/009 1-7613(1982)10<611:petian>2.0.co;2

Tapponnier, P., Xu, Z. Q., Roger, F., et al., 2001. Oblique Stepwise Rise and Growth of the Tibet Plateau. *Science*, 294(5547): 1671–1677. https://doi.org/10.1126/science.105978

Wang, S. F., Fan, C., Wang, G., et al., 2008. Late Cenozoic Deformation along the Northwestern Continuation of the Xianshuihe Fault System, Eastern Tibetan Plateau. *Geological Society of America Bulletin*, 120(3/

4): 312–327. https://doi.org/10.1130/b25833.1

Wang, S. Y., Zhou, R. J., Liang, M. J., et al., 2021. Co-Seismic Surface Rupture and Recurrence Interval of Large Earthquakes along Damaoyaba-Litang Segment of the Litang Fault on the Eastern Margin of the Tibetan Plateau in China. *Journal of Earth Science,* 32(5): 1139–1151. https://doi.org/10.1007/s12583-021-1425-z

Wang, E., Burchfiel, B., 2000. Late Cenozoic to Holocene Deformation in Southwestern Sichuan and Adjacent Yunnan, China, and Its Role in Formation of the Southeastern Part of the Tibetan Plateau. *Geological Society of America Bulletin*, 112(3): 413–423. https://doi.org/10.1130/0016-7606(2000)112<413:lcthdi>2.0.co;2

Wang, Y., Amundson, R., Trumbore, S., 1996. Radiocarbon Dating of Soil Organic Matter. *Quaternary Research*, 45(3): 282–288. https://doi.org/10.1006/qres.1996.0029

Xie, Z. J., Zheng, Y., Liu, C. L., et al., 2017. An Integrated Analysis of Source Parameters, Seismogenic Structure, and Seismic Hazards Related to the 2014 *M*s6.3 Kangding Earthquake, China. *Tectonophysics*, 712/713(9): 1–9. https://doi.org/10.1016/j.tecto.2017.04.030

Yan, B., Jia, D., Lin, A. M., 2018. Late Pleistocene-Holocene Tectonic Landforms Developed along the Strike-Slip Xianshuihe Fault Zone, Tibetan Plateau, China. *Journal of Geodynamics*, 120(6314): 11–22. https://doi.org/10.1016/j.jog.2018.05.005

Yan, B., Wang, M. M., Dong, J., et al., 2019. Investigation and Magnitude Re-Evaluation of the 1955 Zheduotang Earthquake, Eastern Tibetan Plateau, China. *Geological Journal*, 55(11): 7272–7284. https://doi.org/10.1002/gj.3628

Yin, A., 2010. Cenozoic Tectonic Evolution of Asia: A Preliminary Synthesis. *Tectonophysics*, 488(1–4): 293–325. https://doi.org/10.1016/j.tecto.2009.06.002

Yin, A., 2006. Cenozoic Tectonic Evolution of the Himalayan Orogen as Constrained by Along-Strike Variation of Structural Geometry, Exhumation History, and Foreland Sedimentation. *Earth-Science Reviews*, 76(1–2): 1–131. https://doi.org/j.earscirev.2005.05.004

Yang, W., Cheng, J., Liu, J., et al., 2015. The Kangding Earthquake Swarm of November, 2014. *Earthquake Science*, 28(3): 197–207. https://doi.org/10.1007/s11589-015-0123-2

Zhang, H., Shi, Y. L., Wu, Z. L., 2009. A Framework of Massively Parallel Analysis of Regional Earthquake Activities. *Acta Geologica Sinica-English Edition*, 83(4): 786–800. https://doi.org/10.1111/j.1755-6724.2009.00102.x

Zhang, S. M., Xie, F. R., 2001. Seismo-Tectonic Divisions of Strong Earthquakes with *M*s≥7.0 and Their Tectonic Geomorphology along Xianshuihe-Xiaojiang Fault Zone. *Acta Seismologica Sinica*, 14(1): 38–48. https://doi.org/10.1007/s11589-001-0159-3

Zhang, Y. Z., 2015. Tectonic Chronology Constraint on the Main Faults Bounding the East Sichuan-Yunnan Block and Implications for Tibetan Plateau Kinetics: [Dissertation]. China University of Geosciences, Wuhan (in Chinese with English Abstract)

Zhang, Y. Z., Replumaz, A., Leloup, P. H., et al., 2017. Cooling History of the Gongga Batholith: Implications for the Xianshuihe Fault and Miocene Kinematics of SE Tibet. *Earth and Planetary Science Letters*, 465(10): 1–15. https://doi.org/10.1016/j.epsl.2017.02.025

Zhou, R. J., He, Y. L., Huang, Z. Z., et al., 2001. The Slip Rate and Strong Earthquake Recurrence Interval on the Qianning-Kangding Segment of the Xianshuihe Fault Zone. *Acta Seismologica Sinica*, 14(3): 263–273. https://doi.org/10.1007/s11589-001-0004-8